Calculation of cerium and lanthanum anomalies in geological and environmental samples

Barrat Jean-Alix [1, 2, *], Bayon Germain [3], Lalonde Stefan [4]

[1] Univ Brest, CNRS, LEMAR, Institut Universitaire Européen de la Mer (IUEM), Place Nicolas Copernic, 29280 Plouzané, France
[2] Institut Universitaire de France, France
[3] Univ Brest, CNRS, Ifremer, Geo-Ocean, F-29280 Plouzané, France
[4] Univ Brest, CNRS, Ifremer, Geo-Ocean, F-29280 Plouzané, France

* Corresponding author : Jean-Alix Barrat, email address : barrat@univ-brest.fr

Abstract :

The determination of La and Ce anomalies in natural waters, biological samples and biogenic sedimentary rocks can provide unique information on biogeochemical processes in Earth surface environments. Over the last decades, several approaches have been used for calculating La/La* and Ce/Ce*, based on the comparison between measured and theoretical abundances (La* and Ce*) extrapolated from neighboring rare earth element concentrations normalized to chondritic or shale reference values. These extrapolations can be achieved either linearly or semi-logarithmically ("geometrically"), both methods being used in the literature in the absence of any consensus. We show here, using a database of rocks exhibiting no La and Ce anomaly, that the linear extrapolation of La and Ce abundances can result in markedly different results depending on whether chondritic or shale values are used for normalization. The geometric extrapolation allows consistent calculation of La and Ce anomalies for the entire compositional range tested in this study, regardless of whether data are normalized to chondritic or shale reference values. The differences between linear and geometric extrapolations are illustrated by a few selected examples from the literature, including various carbonate rock and seawater samples, further demonstrating that linear extrapolation can result in erroneous estimates of La and Ce anomalies. We thus propose that La/La* and Ce/Ce* ratios in all geological and environmental samples should be determined using the geometric extrapolation only.

Graphical abstract
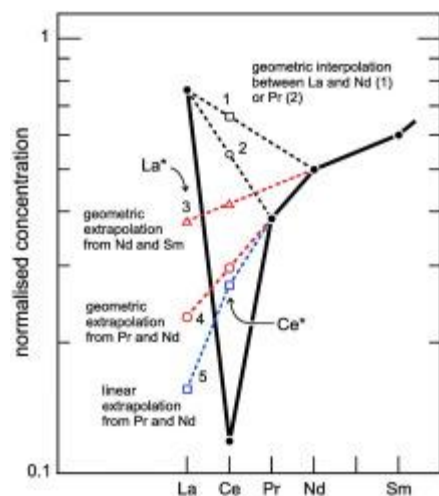
Highlights

► La/La* and Ce/Ce* ratios calculated with linear and geometric extrapolations are compared. ► Linear extrapolation can result in aberrant estimates of La and Ce anomalies. ► La/La* and Ce/Ce* ratios should be determined using the geometric extrapolation only.

Keywords : Rare earth elements, La anomaly, Ce anomaly, Linear extrapolation, Geometric extrapolation

1/ Introduction

Over the last sixty years, rare earth elements (REE) have become one of the most studied groups of elements in Earth sciences. These elements have the particularity of having an extremely coherent geochemical behavior that can be classically described with the "Masuda-Coryell plots" (Masuda, 1962; Coryell et al., 1963), known today as "rare earth patterns". The principle of these diagrams is simple. Rare earth elements are ordered by increasing atomic number, and their abundances in any given sample are normalized to a set of reference values that generally correspond to average concentrations for chondrites (e.g., Anders and Grevesse, 1989; Pourmand et al., 2012; Barrat et al., 2012; Palme et al., 2014) or shales (e.g., Nance and Taylor, 1976; Pourmand et al., 2012; Bau et al., 2018). The first advantage of these diagrams is that the Oddo-Harkins effect (i.e. chemical elements with even atomic numbers are more abundant than adjacent odd atomic number elements) disappears with normalization. Smooth REE patterns are generally obtained for most geological and environmental samples, mostly because all REE are trivalent and not significantly decoupled from each other under relevant physico-chemical conditions. There are notable exceptions, however. For instance, europium (Eu^{2+} and Eu^{3+}) and cerium (Ce^{3+} and Ce^{4+}) can be found in two valence states in geological samples. During particular magmatic or environmental processes, these two elements can be significantly decoupled from their neighboring REE, thereby producing specific elemental depletion or enrichment in normalized REE patterns. Additionally, significant anomalies in La, Sm, Gd and Tm can be also found in terrestrial rocks or natural waters, unrelated to any effect of valence. The occurrence of Tm anomalies in terrestrial rocks are thought to be inherited from the building blocks that formed our planet (Dauphas and Pourmand, 2015; Barrat et al., 2016). The origin of other anomalies is not always well understood, except when they are the result of environmental pollution (e.g., Bau and Dulski, 1996b; Kulaksiz and Bau, 2007, 2013; Merschel and Bau, 2015; Ma et al., 2019; Le Goff et al., 2019, Valdés-Vilchis, 2021).

Among these anomalies, Ce anomalies have received considerable interest. The distinctive behavior of Ce in the marine environment was discovered more than 50 years ago (e.g., Goldberg et al., 1963). The first reliable REE analyses of seawater, various authigenic phases, and ichtyoliths showed very early on that aqueous phases, marine carbonates and other seawater archives could display pronounced negative Ce anomalies (e.g., Piper, 1974; Elderfield and Pagett, 1986 and references therein). The role of Fe and Mn oxides in the development of these anomalies was subsequently proposed because Mn-rich nodules and

74 crusts displayed complementary positive anomalies in Ce (e.g., Goldberg et al., 1963; Piper,

75 1974). Today, it is generally well accepted that the decoupling of Ce from other REEs in the

76 oceans, or more generally in aqueous environments, mainly results from oxidative scavenging

77 of Ce by Fe and Mn hydroxides (e.g., Bau and Koschinsky, 2009). The occurrence of Ce

78 anomalies in natural waters and in the biogenic or authigenic phases that precipitate from

79 them is used as a proxy for oxidative conditions in Earth surface environments (e.g., German

80 and Elderfield, 1990; German et al., 1991; Bau et al., 1997; Wallace et al., 2017; Bellefroid et

81 al., 2018). Cerium anomalies are also of interest for magma-related studies, although their

82 application to basalts and other igneous rocks remains limited. Lavas from subduction zones

83 and oceanic islands occasionally show negative Ce anomalies, interpreted as reflecting a

84 recycled sedimentary component in their mantle sources (e.g., Shimizu et al., 1992; Class and

85 Le Roex, 2008). In contrast, zircons frequently show excess Ce (Ce^{4+} having the same ionic

86 radius as Zr^{4+}), indicating preferential selective incorporation of Ce relative to neighboring

87 REE during crystal growth. The resulting positive Ce anomalies could reflect the Ce^{4+}/Ce^{3+}

88 ratios of their parental magmas, and therefore provide constraints on oxygen fugacity (e.g.,

89 Burnham and Berry, 2012; Trail et al., 2012; Smythe and Brenan, 2016).

90   Unlike Ce, the La anomaly in geological and environmental samples has received

91 much less attention. Lanthanum anomalies represent a common feature in seawater and

92 marine authigenic phases (e.g., Elderfield, 1988; Tostevin et al., 2016), but remains to date

93 undocumented in igneous rocks. The cause of these anomalies is still poorly understood but

94 could relate to the higher stability of La in solution relative to the other light REE (De Baar et

95 al., 1985, Byrne and Kim, 1990, Byrne et al., 1996). Previous studies have suggested that

96 marine barite could play a role in the development of La anomalies in seawater (Grenier et al.,

97 2018). Indeed, Hein et al. (2007) have reported positive La anomalies in this phase. It is likely

98 that the La excesses they measured, however, are analytical artefacts generated in the plasma,

99 notably isobaric interferences from Ba (e.g., $^{138}BaH^+$ on $^{139}La^+$), and need to be confirmed.

100 Recently, a number of pioneering studies have demonstrated that biological activity can also

101 fractionate light-REE (e.g., Pol et al., 2014; Semrau et al., 2018; Bayon et al., 2020a). Wang

102 et al. (2020) reported positive La anomalies in methanotrophic mussels at submarine methane

103 seeps, interpreted as resulting from microbial enzymatic activity related to aerobic methane

104 oxidation. These results ~~have~~ suggested that the La anomaly could serve as a diagnostic tool

105 for tracing past biological activity related to aerobic methanotrophy. Moreover, La also

106 represents an emerging pollutant in modern environments due to its widespread industrial use

107 in magnetic alloys and catalysts for gasoline engines (Kulaksiz and Bau, 2013; Merschel and

108 Bau, 2015). The emergence of anthropogenic La issues in Earth surface environments calls

109 for a better understanding of the mechanisms that control the decoupling of La from

110 neighboring REE in aquatic environments.

111   Over the last few decades, different methods have been proposed for calculating La

112 and Ce anomalies in geological and environmental samples, yet no consensus exists among

113 geochemists on best practices for these calculations. In the literature, historical conventions or

114 habits prevail. These anomalies are calculated from normalized concentrations and by

115 interpolating or extrapolating La and Ce concentrations (La* and Ce*) assuming smooth REE

116 patterns with linear or logarithmic scales. This results in anomaly values that can be very

117 different from one study to another and cannot be compared. Here we show that some

118 commonly used approaches for calculating La and Ce anomalies can lead to aberrant results,

119 hence our call for a standardization of the calculation.

120

121 2/ The different ways to calculate La and Ce anomalies

122 2.1/ Normalization values

123   The patterns of average CI chondrites and average shales do not show significant

124 anomalies in La and Ce when normalized to each other. Therefore, one would expect to

125 calculate similar La/La* or Ce/Ce* values in any given sample following normalization to

126 either chondritic or shale reference values. We will see below that this is not necessarily the

127 case. In this work, we used the average of the Orgueil chondrite concentrations measured by

128 Barrat et al. (2012), and the Post Archean Australian Shale (PAAS) average obtained by

129 Pourmand et al. (2012), which was recalculated relative to our standard values to correct for a

130 slight calibration bias (Barrat et al., 2020). These preferred normalization values are given in

131 Table 1. In the following, X_{CI} and X_{SN} corresponds to the element X concentrations

132 normalized to chondritic or shales values, respectively.

133

134 2.2/ The calculation of Ce and La anomalies

135   By definition, an anomaly visualized in a normalized-REE diagram for an element (X)

136 can be quantified by dividing its measured abundance by its theoretical concentration in the

137   absence of any anomaly (X*). This latter can be calculated by interpolation or extrapolation

138   using the normalized abundances of neighboring elements, assuming a smooth REE pattern.

139   The measured/theoretical elemental ratio (X/X*) thus makes it possible to quantitatively

140   measure a positive (X/X*>1) or a negative (X/X*<1) anomaly for this element.

141   Many approaches to calculating Ce* and La* have been proposed in the last few

142   decades. In the case of magmatic rocks or zircons, which are devoid of La anomalies, Ce* is

143   given by the geometric mean of the normalized concentrations of La and Pr, or interpolated

144   "semi-logarithmically" between La and Nd when Pr abundances are not determined:

145    $$Ce/Ce* = Ce_{CI}/(La_{CI} \times Pr_{CI})^{1/2} \quad (1)$$

146   or

147    $$Ce/Ce* = Ce_{CI}/(La_{CI}^{2/3} \times Nd_{CI}^{1/3}) \quad (2)$$

148

149   The choices of a geometric mean or the semi-log interpolation are justified here by the

150   fact that the REE patterns are plotted in semi-log diagrams, where linear abscissa correspond

151   to the number of protons (Z) of REE and ordinates refer to normalized concentrations

152   conventionally displayed in logarithmic scale.

153   During the 1970s, new developments in sedimentary geochemistry were accompanied

154   by increasing use of reference shale values for normalizing measured REE abundances (e.g.,

155   Piper, 1974). In these early studies, Ce* was interpolated as described above (e.g., Piper

156   (1974) with Equation 2) but also linearly, considering that shale-normalized REE patterns

157   were sometimes plotted using linear scales for both ordinates and abscissae. Additionally,

158   prior to the 1990s and the advent of ICP-MS, REE abundances were mostly measured by

159   neutron activation and Pr concentrations were rarely determined, meaning that Ce* was

160   generally interpolated between La and Nd (e.g., Elderfield and Greaves, 1981), and

161   occasionally between La and Sm (Toyoda et al., 1990):

162    $$Ce/Ce* = 3 \, Ce_{SN}/(2 \, La_{SN} + Nd_{SN}) \qquad (3)$$

163    $$Ce/Ce* = 5 \, Ce_{SN}/(4 \, La_{SN} + Sm_{SN}) \qquad (4)$$

164   It was only with the development of plasma source mass spectrometry in the mid-

165   1980's that the simultaneous determination of the concentrations of all the REE's in a given

166   sample became routine, and the number of analyses that also included Pr increased

167 exponentially. The calculation of the Ce anomaly with Ce* linearly interpolated between La
168 and Pr, is given by the following equation (e.g., De Baar et al., 1983):

$$Ce/Ce* = 2\, Ce_{SN}/(La_{SN} + Pr_{SN}) \qquad (5)$$

170   However, many natural waters, biogenic or authigenic precipitates, and biogenic
171 sediments display La anomalies, thereby biasing the determination of the Ce anomaly using
172 the above formula. With this approach, the calculation of Ce* calculated with La abundances
173 using either linear or geometrical interpolations (Fig. 1) resulted in biased results, generating
174 for instance Ce/Ce* ratios < 1 even in the case of samples devoid of any Ce anomaly. For this
175 reason, Bau and Dulski (1996a) developed a Ce/Ce* vs. Pr/Pr* diagram (Fig. 2, with Ce*
176 linearly interpolated between La and Pr (equation 5), and Pr* linearly interpolated between Ce
177 and Nd, $Pr*_{SN} = (Ce_{SN} + Nd_{SN})/2$). This plot can be used to identify whether La anomalies are
178 present or not, and whether Ce/Ce* ratios < 1 correspond to true negative Ce anomalies or
179 not. This diagram, which was also popularized by Webb and Kamber (2000), is frequently
180 used today. We will come back to it later.

181   Since one cannot properly interpolate Ce* using La with Pr or Nd abundances, one can
182 instead extrapolate Ce* and La* with Pr and Nd abundances (Fig. 1). To avoid ambiguity, we
183 use here the symbols X^{*g} and X^{*l} for the geometric (semi-log) and linear extrapolations,
184 respectively, of the theoretical concentrations of X. The following equations give La_{SN}^{*g},
185 Ce_{SN}^{*g}, La_{SN}^{*l}, and Ce_{SN}^{*l} [e.g., Bolhar et al. (2004) for the linear interpolations and Lawrence
186 et al. (2006) for the geometric interpolations], and of course similar equations can be written
187 for the chondritic normalization:

$$La_{SN}^{*g} = Pr_{SN}^{3}/Nd_{SN}^{2} \qquad (6)$$

$$Ce_{SN}^{*g} = Pr_{SN}^{2}/Nd_{SN} \qquad (7)$$

$$La_{SN}^{*l} = 3\, Pr_{SN} - 2\, Nd_{SN} \qquad (8)$$

$$Ce_{SN}^{*l} = 2\, Pr_{SN} - Nd_{SN} \qquad (9)$$

193   These are the equations used by most teams working today on sedimentary rocks or
194 natural waters, without consensus on whether geometric or linear interpolations should be
195 used or not. Questions arise about whether linear or geometric extrapolation allows for a

196 better estimation of the anomalies. Additionally, do the normalization values (chondrite or
197 shale) lead to different estimates of La and Ce anomalies?

198

199 2.3/ Which type of extrapolation to select?

200   An ideal extrapolation should meet the following criteria:

201 - To allow for the best estimation of La* and Ce* concentrations;

202 - To be universal, i.e. to correctly estimate La* and Ce* over the entire compositional range
203 encountered in Earth systems;

204 - To be independent of normalization values; in other words, the type of extrapolation must be
205 able to calculate consistent La/La* or Ce/Ce* ratios even if the data are normalized to
206 chondritic or shale values.

207   We have built a database including a total of 286 magmatic rocks, covering a large
208 range of light-REE depletion or enrichment, in order to evaluate the ability of both linear and
209 geometric extrapolations to meet these requirements (Hamelin et al., 2009, 2010; Cordier et
210 al., 2010; Daoud et al., 2010; Pelleter et al., 2014; Barrat et al., 2016; Caroff et al., 2021,
211 Pelleter et al., 2014). The chosen suite of igneous rocks ranges from highly-depleted MORBs
212 to highly-enriched alkaline rocks through lamprophyres, and some evolved rocks [$(La/Sm)_{CI}$
213 = 0.24 - 13.4]. All of these rocks were analyzed using the same procedure and calibration to
214 avoid any potential analytical bias (e.g., Barrat et al., 2012). Based on replicate analyses of
215 standard reference materials and samples (e.g., Barrat et al., 2012, 2016, 2020; Charles et al.,
216 2021), the precision for abundances is typically much better than 5 %, and 3 % for element
217 ratios (one relative standard deviation - RSD), including La/La* and Ce/Ce*. Finally, and
218 obviously most importantly, these rocks do not have Ce, nor La anomalies: their "correct"
219 La/La* or Ce/Ce* ratios are hence ~1.

220   We calculated the Ce/Ce* ratio with Ce* interpolated geometrically between La and
221 Pr (equation 1) for the rocks in our database. This ratio varies from 0.92 to 1.11 only, with
222 most of the samples exhibiting Ce/Ce* between 0.95 and 1.05, confirming the lack of
223 significant Ce anomaly (Fig. 2a). The curvature of some of the patterns is largely responsible
224 for this range. In the $Ce_{SN}/Ce_{SN}*$ vs. $Pr_{SN}/Pr_{SN}*$ plot of Bau and Dulski (1996), where Ce* and
225 Pr* are linearly interpolated, only half of studied rock samples are located in the panel

226   attributed to samples having no Ce and La anomalies; the other half being scattered in an area

227   corresponding to positive anomalies in Ce with either positive or negative La anomaly. This

228   discrepancy is somewhat surprising, as one would have expected the vast majority of studied

229   rocks to fall within the area corresponding to samples having no anomalies. This is not related

230   to the accuracy of the analyses used (< 2% (1 RSD) for the $Ce_{SN}/Ce_{SN}*$ and $Pr_{SN}/Pr_{SN}*$ – the

231   reader is referred to Barrat et al. (2016, 2020) and Charles et al. (2021) for examples of results

232   obtained on various types of standards). This can be explained, among other things, by the

233   fact that the rocks used in our database display a much greater LREE compositional range

234   relative to those used by Bau and Dulski (1996), and by the poor approximations of Ce* and

235   Pr* by linear interpolations when the patterns are highly fractionated (here, the samples that

236   deviate most from the expected area, are the most light-REE-depleted ones).

237   Next, we use Ce/Nd vs. Pr/Nd plots to compare linear or semi log extrapolations for

238   Ce, normalizing ratios to either chondritic (Fig. 3a) or PAAS values (Fig. 3b). Indeed, the

239    $Ce*^g/Nd$ and $Ce*^l/Nd$ ratios define parabolas and straight lines in these plots, respectively:

240        $$Ce_{CI}*^g/Nd_{CI} = (Pr_{CI}/Nd_{CI})^2 \text{ and } Ce_{SN}*^g/Nd_{SN} = (Pr_{SN}/Nd_{SN})^2 \qquad (10)$$

241        $$Ce_{CI}*^l/Nd_{CI} = 2\,(Pr_{CI}/Nd_{CI}) - 1 \text{ and } Ce_{SN}*^l/Nd_{SN} = 2\,(Pr_{SN}/Nd_{SN}) - 1 \qquad (11)$$

242   The rocks of our database having no Ce anomaly, they can be directly compared to

243   these curves or lines. Figure 3 shows directly that the parabolas calculated using a geometric

244   extrapolation reproduce very satisfactorily the Ce/Nd ratios of the rocks over the whole range

245   of Pr/Nd ratios considered in this study. On the other hand, the lines corresponding to the

246   linear extrapolation allow for an acceptable approximation of Ce* in a given range of values

247   only. Note that in each diagram the parabola and the line are tangent to the point (1,1). If we

248   consider that both interpolations give acceptable results when $Ce*^g/Ce*^l$ is between 1 and

249   1.05, we can easily calculate that we can then use indifferently one or the other extrapolation

250   only when $(Pr/Nd)_{CI}$ or $(Pr/Nd)_{SN}$ are between 0.82 and 1.28. Whenever $(Pr/Nd)_{CI}$ or

251    $(Pr/Nd)_{SN}$ plot outside this range of values, the $Ce/Ce*^l$ and $Ce/Ce*^g$ ratios diverge, due to a

252   clear underestimation of $Ce*^l$. The choice of normalization values is not without consequence

253   if linear extrapolation is used. The use of shales instead of chondritic reference values results

254   in a shift towards the left of the diagram [because $(Pr/Nd)_{SN}<(Pr/Nd)_{CI}$], and, as a

255   consequence, the $Ce_{CI}/Ce_{CI}*^l$ and $Ce_{SN}/Ce_{SN}*^l$ ratios may be very different depending on the

256   Pr/Nd ratios. In this study, this is strikingly illustrated by the fact that the $Ce_{CI}/Ce_{CI}*^l$ ratio

257   varies from 0.91 to 1.24 only, while $Ce_{SN}/Ce_{SN}*^l$ varies from 0.96 to 5.11. On the other hand,

258   the $Ce_{SN}/Ce_{SN}*^g$ and $Ce_{CI}/Ce_{CI}*^g$ ratios are perfectly proportional, with

259    $(Ce_{SN}/Ce_{SN}*^g)/(Ce_{CI}/Ce_{CI}*^g)$ being equal to the PAAS $Ce_{CI}/Ce_{CI}*^g$ ratio.

260   In Fig. 4, we show the $Ce/Ce*^g$ and $Ce/Ce*^l$ ratios obtained after normalization to

261   either chondritic or PAAS values. The diagrams not only indicate that the ranges of values

262   obtained are different, but that the correlations are poor: Ce anomalies calculated in different

263   ways are not comparable.

264   We followed the same approach for La anomalies. In La/Nd vs. Pr/Nd plots, the

265    $La*^g/Nd$ and $La*^l/Nd$ ratios define cubic curves and straight lines, respectively:

266        $$La_{CI}*^g/Nd_{CI} = (Pr_{CI}/Nd_{CI})^3 \text{ and } La_{SN}*^g/Nd_{SN} = (Pr_{SN}/Nd_{SN})^3 \qquad (12)$$

267        $$La_{CI}*^l/Nd_{CI} = 3 (Pr_{CI}/Nd_{CI}) - 2 \text{ and } La_{SN}*^l/Nd_{SN} = 3 (Pr_{SN}/Nd_{SN}) - 2 \qquad (13)$$

268   As shown above, the curves corresponding to the geometric extrapolation superimpose

269   well on the correlation trends displayed by the rock data used in this study (Fig. 5). The

270   straight lines corresponding to the linear extrapolation only allow a good estimation of the

271   La/Nd ratios for the patterns exhibit little REE decoupling (i.e., when $(Pr/Nd)_{CI}$ or $(Pr/Nd)_{SN}$

272   close to 1). Calculation of La anomalies using the linear extrapolation even appears to be

273   inconsistent for many samples. When the data are normalized to chondritic reference values,

274   the linear extrapolation underestimates considerably La* values, leading to anomalously high

275    $La/La*^l$ ratios. The situation is much more problematic when data are normalized to PAAS

276   values, especially for the most light-REE depleted samples. Not only does Equation 8

277   underestimate $La_{SN}*$, but when $(Pr/Nd)_{SN} \leq 2/3$, $La_{SN}*^l \leq 0$ and the $La_{SN}/La_{SN}*^l$ ratio becomes

278   negative or tends toward $-\infty$ when $(Pr/Nd)_{SN}$ is just below 2/3. The $La_{SN}/La_{SN}*^l$ ratio also

279   tends toward $+\infty$ when $(Pr/Nd)_{SN}$ is just above 2/3. These cases are not uncommon on Earth:

280   the $La_{SN}/La_{SN}*^l$ ratios calculated with our database range from -216.3 to 103.5, while much

281   smaller ranges around 1 are obtained with other La/La* calculations (Fig. 6). As for the Ce

282   anomaly, the ratios $La_{SN}/La_{SN}*^g$ and $La_{CI}/La_{CI}*^g$ are perfectly proportional, and the $La/La*^g$

283   and $La/La*^l$ ratios are not strongly correlated, even when the latter ratios are not aberrant. The

284   range of $(Pr/Nd)_{SN}$ ratios for which La anomaly calculations are similar for linear or

285   geometric interpolations $(La*^g/La*^l<1.05)$ is narrow and only between 0.9 and 1.16.

286   These results demonstrate that La and Ce anomalies calculated using linear

287   extrapolation can lead to biased or even aberrant values in many cases. Moreover, the

288   calculated anomalies are very dependent on the type of normalization used. On the other

289   hand, the results obtained with our database indicate that the use of geometric extrapolation
290   results in more reliable estimates of La and Ce anomalies, regardless of whether chondrite or
291   shale are used for normalization, and this applies for the whole range of compositions tested
292   in this study.

293

3/ Some examples

295   The theoretical ground discussed above is illustrated below for a few examples taken
296   from the literature (Table 1). It is not our goal here to discuss the differences obtained
297   between the anomalies calculated for each type of rocks or waters, normalizations and
298   extrapolations. We have chosen to discuss in more detail specific cases of seawater and
299   biogenic carbonates in order to show how the choice of extrapolation can affect data
300   interpretation.

301

3.1. Carbonates

303   We selected 6 series of carbonate samples corresponding to microbialites or
304   stromatolites of different ages: the 3.45-Ga-old Strelley Pool stromatolites (Van Kranendonk
305   et al., 2003); the 2.84-Ga-old Mushandike stromatolites (Kamber et al, 2004); the 2.7-Ga-old
306   Fortescue stromatolites (Bohlar and Van Kranendonk, 2007); the 2.52-Ga-old Campbellrand
307   stromatolites (Kamber and Webb, 2001); the late Devonian reefal carbonates from the
308   Lennard Shelf (Nothdurft et al., 2004); and the Holocene microbialites from the Heron Reef
309   (Webb and Kamber, 2000). All data used here were obtained in the same laboratory
310   (ACQUIRE, Brisbane) following similar analytical procedures, and are of excellent quality.
311   These series of samples do not of course cover the full compositional range existing for these
312   types of carbonates, but nevertheless display important variations in various REE signatures.

313   We plotted these analyses in the Ce/Ce* vs. Pr/Pr* diagram of Bau and Dulski
314   (1996a), which can be used, as discussed above, to identify the presence of Ce and La
315   anomalies (Fig. 7a). In this diagram, Ce* and Pr* are linearly interpolated between La and Pr
316   and Ce and Nd respectively. All but 3 samples have a Ce/Ce* ratio<1 when calculated in this
317   way, but only those with a Pr/Pr* ratio >1 have a true negative Ce anomaly, due to the bias
318   introduced by the La anomalies.   We calculated the Ce and La anomalies using both
319   geometrical and linear extrapolation from PAAS-normalized concentrations. The obtained

320 $Ce_{SN}/Ce_{SN}*^g$ and $Ce_{SN}/Ce_{SN}*^l$ ratios are very similar (Fig. 8a) for most samples. Only 4

321 samples from Strelley Pool deviate significantly from the trend, their $Ce_{SN}*^l$ certainly being

322 underestimated. The $La_{SN}/La_{SN}*^g$ and $La_{SN}/La_{SN}*^l$ ratios are for most samples reasonably well

323 correlated, but the Holocene samples markedly deviate from the trend with $La_{SN}/La_{SN}*^l$ ratios

324 greater than $La^{SN}/La_{SN}*^g$, and 4 Strelley Pool samples display outlier $La_{SN}/La_{SN}*^l$ values (=-

325 27.7 to -4.6). These calculations show that in many cases, one can use either linear or

326 geometric extrapolations to estimate La or Ce anomalies, without detecting an anomaly. This

327 is particularly the case when the patterns are little or not fractionated, but linear extrapolation

328 can nevertheless generate artifacts or even aberrant values. To avoid the latter, we recommend

329 using only the geometrical extrapolation to calculate La or Ce anomalies.

330 Although the Ce/Ce* vs. Pr/Pr* diagram proposed by Bau and Dulski (1996a) can

331 bring useful insights for discussing REE patterns and the origin of La and Ce anomalies, it

332 also suffers from inherent drawbacks that are briefly described below:

333 - The Ce/Ce* ratio used in this diagram depends on a Ce* value linearly interpolated

334 between La and Pr. This ratio does not allow a correct quantification of the anomaly, because

335 in addition to the problems related to the linear interpolation, it can be largely biased for the

336 samples with an anomaly in La, as already reported by these authors

337 - the Pr/Pr* ratio allows for the detection of samples with positive or negative

338 anomalies in La, but does not allow the quantification of the latter.

339 For all the above-mentioned reasons, we propose using instead the $Ce/Ce*^g$ vs.

340 $La/La*^g$ diagram, which is better suited for illustrating whether any given sample displays La

341 or Ce anomalies, and which also provides direct quantification of these anomalies.

342 Additionally, the use of the geometric extrapolation ensures that calculated anomalies in this

343 diagram are independent of the type of reference used for normalization, and above all it

344 avoids the calculation of erroneous Ce/Ce* or La/La* ratios due to artifacts linked to linear

345 extrapolation. For the carbonate samples selected here, the $Ce/Ce*^g$ vs. $La/La*^g$ diagram

346 shows that these carbonates exhibit a wide range of positive La anomalies, but also allows one

347 to identify a clear distinction between those Archean samples characterized by the absence of

348 marked negative Ce anomalies ($Ce/Ce*^g \geq 1$), in contrast with the Devonian or Holocene

349 carbonates.

350

3.2. Seawater

We employ here a previously published REE database for seawater samples (n=1649; Bayon et al., 2020b). We normalized the concentrations with PAAS and examined $(Ce/Nd)_{SN}$ and $(La/Nd)_{SN}$ vs. $(Pr/Nd)_{SN}$ systematics (Fig. 9). The $(Pr/Nd)_{SN}$ ratios range from 0.49 to 1.19: 62% of the analyses have $(Pr/Nd)_{SN}$ ratios <0.82, and thus have $Ce/Ce*^{l}$ and $Ce/Ce*^{g}$ ratios that differ by more than 5%; 97% of the analyses have $(Pr/Nd)_{SN}$ ratios<0.9, and thus have $La/La*^{l}$ and $La/La*^{g}$ ratios that differ by more than 5%. The position of the points with respect to the calculated curves and lines shows unambiguously that the choice of the extrapolation method is critical here, as the $La*^{l}$ or $Ce*^{l}$ concentrations are most often underestimated by the calculation, or even aberrant ($La*^{l}$<0 for many samples).

In order to illustrate the pitfalls of using the linear extrapolation for the case of seawater samples, we chose two hydrographic stations from the China Sea (Alibo and Nozaki, 2000) and the Kerguelen Plateau (Grenier et al., 2018), and examined the vertical profiles of La anomalies calculated by normalizing the data with respect to both CI-chondrite and PAAS, extrapolating La* linearly or geometrically (Fig. 10). For both stations, $La_{SN}/La_{SN}*^{l}$ ratios are always much larger than those estimated geometrically by normalizing with PAAS or with CI-chondrite: for the first station, $La_{SN}/La_{SN}*^{l}$ ratios are 1.30 to 1.42 times larger than $La_{SN}/La_{SN}*^{g}$ ratios, and for the second station they are 1.54 to 3.71 times larger. The La anomalies estimated with the $La_{SN}/La_{SN}*^{l}$ ratios are obviously strongly exaggerated, and these calculations must be rejected. Note that the $La_{CI}/La_{CI}*^{l}$ ratios are very close to the $La_{CI}/La_{CI}*^{g}$ or $La_{SN}/La_{SN}*^{g}$ ratios, and similar or identical profiles are obtained with these three ratios. These results adds further support that the use of geometric extrapolation is best suited for calculating La and Ce anomalies relative to the linear extrapolation. The fact that the $La_{CI}/La_{CI}*^{l}$ ratios are correct here is fortuitous, and is easily explained. The $(Pr/Nd)_{CI}$ ratios are higher than the $(Pr/Nd)_{SN}$ ratios, and are then in the range of values for which geometric and linear extrapolations give equivalent results.

4/ Conclusion

An extended REE database for a suite of igneous rocks devoid of La and Ce anomalies, was used to investigate the effects of linear and geometric extrapolations for calculating La/La* and Ce/Ce* ratios in geological and environmental samples, based on Pr and Nd concentrations. We show that the linear extrapolation only provides reliable estimates

383 of La* and Ce* for a limited range of REE compositions. These calculations can lead in many

384 cases to biased La/La* and Ce/Ce* values, which are also critically dependent on the type of

385 normalization used (i.e. chondritic versus shale reference values). The artifacts generated

386 when using the linear extrapolation are illustrated with examples from the literature for

387 seawater and biogenic carbonates, demonstrating that it can lead to misleading interpretations

388 regarding the presence and/or significance of La and Ce anomalies. Finally, we show that the

389 use of geometric extrapolation ensures reliable quantitative calculation of Ce and La

390 anomalies in all samples, which remain unaffected by the type of normalization used. We

391 propose that linear extrapolations be discontinued, and instead recommend the exclusive use

392 of geometric extrapolations to quantify La and Ce anomalies.

393

397

References

Alibo, D.S., Nozaki, Y. (2000) Dissolved rare earth elements in the South China Sea: geochemical characterization of the water masses. *J. Geophys. Res.* 105, C12, 28771-28783.

Anders E. and Grevesse N. (1989) Abundances of the elements: meteoritic and solar. *Geochim. Cosmochim. Acta* **53**, 197–214.

Barrat J.A., Zanda B., Moynier F., Bollinger C., Liorzou C., and Bayon G. (2012) Geochemistry of CI chondrites: Major and trace elements, and Cu and Zn isotopes. *Geochim. Cosmochim. Acta* **83**, 79-92.

Barrat J.A., Dauphas N., Gillet P., Bollinger C., Etoubleau J., Bischoff A., Yamaguchi A. (2016) Evidence from Tm anomalies for non-CI refractory lithophile element proportions in terrestrial planets and achondrites. *Geochim. Cosmochim. Acta*, **176**, 1-17.

Barrat J.A., Bayon G., Wang X., Le Goff S., Rouget M.L., Gueguen B., Ben Salem B. (2020) A new chemical separation procedure for the determination of rare earth elements and yttrium abundances in carbonates by ICP-MS. *Talanta* **219**, 121244.

Bau, M., Dulski, P. (1996a) Distribution of yttrium and rare-earth elements in the Penge and Kuruman iron formations, Transvaal Supergroup, South Africa. *Precambrian Res*. **79**, 37–55.

Bau, M., Dulski, P. (1996b) Anthropogenic origin of positive gadolinium anomalies in river waters. *Earth Planet. Sci. Lett.* **143**, 245-255.

Bau M., Romer R.L., Lüders V., Dulski P. (2003) Tracing element sources of hydrothermal mineral deposits: REE and Y distribution and Sr-Nd-Pb isotopes in fluorite from MVT deposits in the Pennine Orefield, England. *Mineralium Deposita* **38**, 992-1008.

Bau M., Koschinsky A. (2009) Oxidative scavenging of cerium on hydrous Fe oxide: Evidence from the distribution of rare earth elements and yttrium between Fe oxides and Mn oxides in hydrogenetic ferromanganese crusts. *Geochem. J.* **43**, 37–47.

Bau M., Schmidt K., Pack A., Bendel B., Kraemer D. (2018) The European Shale: an improved data set for normalization of rare earth elements and yttrium concentrations in environmental and biological samples from Europe. *Applied Geochem.* **90**, 142-149.

Bayon G., Lambert T., Vigier N., De Dekker P., Freslon N., Jang K., Larkin C.S., Piotrovski A.M., Tachikawa K., Thollon M., Tipper E.D. (2020a) Rare earth element and neodymium isotope tracing of sedimentary rock weathering. *Chem. Geol.* **553**, 119794.

Bayon G., Lemaitre N., Barrat J.A., Wang X., Feng D., Duperron S. (2020b) Microbial utilization of rare earth elements at cold seeps related to aerobic methane oxidation. *Chem. Geol.* **555**, 119832.

Bellefroid E.J., Hood A.V.S. , Hoffman P.F., Thomas M.D., Reinhard C.T., Planavsky N.J. (2018) Constraints on Paleoproterozoic atmospheric oxygen levels. *PNAS* **115**, 8104-8109.

Bolhar R., Van Kranendonk M.J. (2007) A non-marine depositional setting for the northern Fortescue Group, Pilbara Craton, inferred from trace element geochemistry of stromatolitic carbonates. *Precambrian Res.* **155**, 229-250.

Bolhar R., Kamber B.S., Moorbath S., Fedo C.M., and Whitehouse, M.J. (2004). Characterisation of early Archaean chemical sediments by trace element signatures. *Earth Planet. Sci. Lett.* **222**, 43-60.

Burnham A.D., Berry A.J. (2012) An experimental study of trace element partitioning between zircon and melt as a function of oxygen fugacity. *Geochim. Cosmochim. Acta* **95**, 196-212.

Byrne R.H., Kim K.H. (1990) Rare earth element scavenging in seawater. *Geochim. Cosmochim. Acta* **54**, 2645-2656.

Byrne R.H., Liu X., and Schijf J. (1996). The influence of phosphate coprecipitation on rare earth distributions in natural waters. *Geochim. Cosmochim. Acta* **60**, 3341–3346.

Caroff M., Barrat J.A., Le Gall B. (2021) Kersantites and associated intrusives from the type locality (Kersanton), Variscan Belt of Western Armorica. *Gondwana Res.* **98**, 46-62.

Cordier C., Benoit M., Hémond C., Dyment J., Le Gall B., Briais A., Kitazawa M. (2010), Time scales of melt extraction revealed by distribution of lava composition across a ridge axis. *Geochem. Geophys. Geosyst.* **11**, Q0AC06,doi:10.1029/2010GC003074.

Charles C., Barrat J.A., Pelleter E. (2021) Trace element determinations in Fe–Mn oxides by high resolution ICP-MS after Tm addition. *Talanta* **233**, 122446.

Class C., Le Roex A.P. (2008) Ce anomalies in Gough Island lavas - Trace element characteristics of a recycled sediment component. *Earth Planet. Sci. Lett.* **265**, 475-486.

Coryell C.D., Chase J. W., and Winchester J.W. (1963) A procedure for geochemical interpretation of terrestrial rare-earth abundance patterns. *J. Geophys. Res.* **68**, 559-566

Cotruvo, jr., J.A. (2019) The chemistry of lanthanides in biology: recent discoveries, emerging principles, and technological applications. *ACS Cent. Sci.* 5, 1496–1506.

Daoud M.A., Maury R.C., Barrat J.A., Taylor R.N., Le Gall B., Guillou H., Cotten J., Rolet J. (2010) A LREE-depleted component in the Afar plume: further evidence from Quaternary Djibouti basalts. *Lithos* **114**, 327-336.

Dauphas N, Pourmand A. (2015) Thulium anomalies and rare earth element patterns in meteorites and Earth: Nebular fractionation and the nugget effect. *Geochim. Cosmochim. Acta* **163**, 234-261.

De Baar H.J.W., Bacon M.P., Brewer P.G. (1983) Rare-earth distributions with a positive Ce anomaly in the Western North Atlantic Ocean. *Nature* **301**, 324-327.

De Baar H.J.W., Bacon M.P., Brewer P.G., and Bruland, K.W. (1985) Rare earth elements in the Pacific and Atlantic oceans. *Geochim. Cosmochim. Acta* **49**, 1943–1959.

Elderfield H. (1988) The oceanic chemistry of the rare-earth elements. *Philosophical Transaction of the Royal Society of London. Series A, Mathematical and Physical Sciences* **325**, 105-126.

Elderfield H., and Greaves M.J. (1981) Negative cerium anomalies in the rare earth element patterns of oceanic ferromanganese nodules. *Earth Planet. Sci. Lett.* **55**, 163-170.

Elderfield H., Pagett R. (1986) Rare Earth elements in Ichthyoliths: variations with redox conditions and depositional environment. In: Riley, J.P. (Ed.), Science of the Total Environment. Elsevier, Amsterdam, pp. 175–197.

German C.R., Elderfield H. (1990) Application of the Ce anomaly as a paleoredox indicator: The ground rules. *Paleoceanography* **5**, 823-833.

German C.R., Holliday B.P., Elderfield H. (1991) Redox cycling of rare earth elements in the suboxic zone of the Black Sea. *Geochim. Cosmochim. Acta* **55**, 3553-3558.

Goldberg E.D., Koide M., Schmitt R.A. (1963) Rare earth distributions in the marine environment. *J. Geophys. Res.* **68**, 4209-4217.

Grenier M, Garcia-Solsona E., Lemaitre N., Trull T.W., Bouvier V., Nonnotte P., Van Beek P., Souhaut M., Lacan F., Jeandel C. (2018) Differentiating lithogenic supplies, water mass transport, and biological processes on and off the Kerguelen Plateau using rare earth element concentrations and neodymium isotopic compositions. *Frontiers in Marine Science* **5**, 426.

509
510 Hamelin C., Seitz H.M., Barrat J.A., Dosso L., Maury R.C., Chaussidon M. (2009) A low δ⁷Li lower crustal
511   component: evidence from an alkalic intraplate volcanic series (Chaîne des Puys, French Massif Central).
512   *Chem. Geol.* **266**, 214-226.

513 Hamelin C., Dosso L., Hanan B., Barrat J.A., Klingelhöfer F., Ondréas H. (2010) Sr-Nd-Hf isotopes along the
514   Pacific Antarctic Ridge from 41 to 53°S. *Geophys Res. Lett.* 37, L10303, doi:10.1029/2010GL042979.
515

516 Hein J. R., Zierenberg R. A., Maynard J. B., and Hannington, M. D. (2007). Multifarious barite-forming
517   environments along a rifted continental margin, Southern California Borderland. Deep-Sea Res. II 54,
518   1327-1349.
519

520 Kamber B.S. and Webb G.E. (2001) The geochemistry of late Archaean microbial carbonate: Implications for
521   ocean chemistry and continental erosion history. *Geochim. Cosmochim. Acta* **65,** 2509–2525.
522

523 Kamber B.S., Bolhar R., Webb G.E. (2004). Geochemistry of late Archaean stromatolites from Zimbabwe:
524   evidence for microbial life in restricted epicontinental seas. *Precambrian Res.* **132**, 379-399.
525

526 Kulaksiz S., Bau M. (2007) Contrasting behaviour of anthropogenic gadolinium and natural rare earth elements
527   in estuaries and the gadolinium input into the North Sea. *Earth Planet. Sci. Lett.* **260**, 361-371.
528

529 Kulaksiz S., Bau M. (2013) Anthropogenic dissolved and colloid/nanoparticle-bound samarium, lanthanum and
530   gadolinium in the Rhine River and the impending destruction of the natural rare earth element distribution
531   in rivers. *Earth Planet. Sci. Lett.* **362**, 43-50.
532

533 Lawrence M.G., Greig A., Collerson K.D., Kamber B.S. (2006) Rare Earth Element and Yttrium variability in
534   South East QueenslandWaterways. *Aquat. Geochem.* **12**, 39–72.
535

536 Le Goff S., Barrat J.A., Chauvaud L., Paulet Y.M., Gueguen B., Ben Salem D. (2019) Compound-specific
537   recording of gadolinium pollution in coastal waters by great scallops. *Scientific Reports* **9**, 8015.
538

539 Ma L., Dang D.H., Wang W., Evans R.D., Wang W.X. (2019) Rare earth elements in the Pearl River Delta of
540   China: Potential impacts of the REE industry on water, suspended particles and oysters. *Environmental*
541   *Pollution* **244**, 190-201
542

543 Masuda A. (1962) Regularities in variation of relative abundances of Lanthanide elements and an attempt to
544   analyse separation index patterns of some minerals. *J. Earth Sci. Nagoya Univ.* **10**, 173-187.
545

546 Merschel G., Bau M. (2015) Rare earth elements in the aragonitic shell of freshwater mussel Corbicula fluminea
547   and the bioavailability of anthropogenic lanthanum, samarium and gadolinium in river water. *Sci. Total*
548   *Environment* **533**, 91-101.
549

550 Nance W.B., Taylor S.R., (1976) Rare earth element patterns and crustal evolution–I. Australian post-Archean
551   sedimentary rocks. *Geochim. Cosmochim. Acta* **40**, 1539–1551.
552

553 Northdurft L.D., Webb G.E., Kamber B.S. (2004) Rare earth element geochemistry of Late Devonian reefal
554   carbonates, Canning Basin, Western Australia: confirmation of a seawater REE proxy in ancient limestones
555   *Geochim. Cosmochim. Acta* **68**, 263-283.

556 Palme H., Lodders K. and Jones A. (2014) Solar System Abundances of the Elements. In: Holland H.D. and
557   Turekian K.K. (eds.) Treatise on Geochemistry, Second Edition, vol. 2, pp. 15-36. Oxford: Elsevier.

558
559 Piper D.Z. (1974a) Rare earth elements in the sedimentary cycle: a summary. *Chem. Geol.* **14**, 285--304.
560

561 Piper D.Z. (1974b) Rare earth elements in ferromanganese nodules and other marine phases. *Geochim.*
562   *Cosmochim. Acta* **38**, 1007–1022.
563

564 Pelleter A.A., Caroff M., Cordier C., Bachelery P., Nehlig P., Debeuf D., Arnaud N. (2014) Melilite-bearing
565   lavas in Mayotte (France): An insight into the mantle source below the Comores. *Lithos* **208-209**, 281-297.
566

Pol, A. *et al.* (2014) Rare earth metals are essential for methanotrophic life in volcanic mudpots. *Environmental Microbiology* **16**, 255–264.

Pourmand, A., Dauphas, N., Ireland, T.J. (2012) A novel extraction chromatography and MC-ICP-MS technique for rapid analysis of REE, Sc and Y: Revising CI-chondrite and Post-Archean Australian Shale (PAAS) abundances. *Chem. Geol.* **291**, 38-54.

Semrau, J.D., DiSpirito, A.A., Gu, W., Yoon, S. (2018) Metals and Methanotrophy. *Appl Environ Microbiol* **84**, e02289-17.

Shimizu H., Sawatari H., Kawata Y., Dunkley P.N., Masuda A. (1992) Ce and Nd isotope geochemistry on island arc volcanic rocks with negative Ce anomaly: existence of sources with concave REE patterns in the mantle beneath the Solomon and Bonin island arcs. *Contrib. Mineral. Petrol.* **110**, 242-252.

Smythe D.J., Brenan J.M. (2016) Magmatic oxygen fugacity estimated using zircon-melt partitioning of cerium. *Earth Planet. Sci. Lett.* **453**, 260-266.

Toyoda K., Nakamura Y., Masuda A., 1990. Rare earth elements of Pacific pelagic sediments. *Geochim. Cosmochim. Acta* **54**, 1093–1103.

Tostevin R., Graham A., Shields G.A., Tarbuck G.M., Tianchen He, Clarkson M.O., Wood R.A. (2016) Effective use of cerium anomalies as a redox proxy in carbonate-dominated marine settings. *Chem. Geol.* **438**, 146-162

Trail D., Watson E.B., Tailby N.D. (2012) Ce and Eu anomalies in zircon as proxies for the oxidation state of magmas. *Geochim. Cosmochim. Acta* **97**, 70-87.

Valdés-Vilchis S., Sànchez-Beristain F., Bernal J.P., Juàrez-Aguilar E.A. (2021) Rare Earth Elements and Yttrium (REE+Y) patterns in recent *Anadara brasiliana* shells from Playa Norte, Barra de Cazones (Veracruz, Mexico): Evidence of anthropogenic contamination linked to river output? *Journal of South American Earth Sciences* **110**, 103368.

Van Kranendonk M.J., Webb G.E., Kamber B.S. (2003) New geological and trace element evidence from 3.45 Ga stromatolitic carbonates in the Pilbara Craton: support of a marine, biogenic origin and for a reducing Archaean ocean. *Geobiology* **1**, 91-108.

Wallace M.W., Hood A.S., Shuster A., Greig A., Planavsky N.J., Reed C.P. (2017) Oxygenation history of the Neoproterozoic to early Phanerozoic and the rise of land plants. *Earth Planet. Sci. Lett.* **466**, 12-19.

Wang X., Barrat J.A., Bayon G., Chauvaud L., Feng D. (2020) Lanthanum anomalies as fingerprints of methanotrophy. *Geochem. Persp. Let.* **14**, 26–30.

Webb G.E., Kamber B.S. (2000) Rare earth elements in Holocene reefal microbialites: a new shallow seawater proxy. *Geochim. Cosmochim. Acta* **64**, 1557-1565.

Table 1. Preferred normalization values and examples of calculation. (References: 1: Barrat et al., 2012; 2: Pourmand et al., 2012, Barrat et al., 2020; 3: Barrat
et al., 2016 ; 4 : Bau et al., 2003 ; 5 : Charles et al., 2021 ; 6 : Van Kranendonk et al., 2003).

	CI-chondrite	CI-chondrite	PAAS	PAAS	MORB	fluorite	Mn-nodule	stromatolite	BIF
ref.	1	1	2	2	3	4	5	6	6
#					PI 18-06	CT2a	GSMC-1	2-9-11a	IF-G
unit	µg/g	µmol/kg	µg/g	µmol/kg	µg/g	µg/g	µg/g	ng/g	ng/g
Y	1.56	17.55	32.2	362		35.6	259	1014.2	9135
La	0.235	1.692	44.75	322.2	0.504	0.54	326	56.3	2706
Ce	0.600	4.28	87.29	623.0	2.13	0.89	1246	85.9	3902
Pr	0.091	0.646	10.1	71.68	0.464	0.23	68.74	14	430
Nd	0.464	3.22	36.98	256.4	3.00	1.42	283	77.7	1731
Sm	0.153	1.018	6.908	45.94	1.30	0.57	58.4	45.9	399
Eu	0.0586	0.386	1.188	7.818	0.582	0.18	14.36	27.1	362
Gd	0.206	1.31	5.958	37.89	2.18	1.33	61.68	89.6	667
Tb	0.0375	0.236	0.894	5.625	0.432	0.23	9.53	13.6	112
Dy	0.254	1.563	5.272	32.44	3.16	1.71	56.48	70	791
Ho	0.0566	0.343	1.078	6.536	0.743	0.4	11.58	17.7	207
Er	0.166	0.992	3.094	18.50	2.23	1.15	31.93	54.8	619
Tm	0.0262	0.155	0.468	2.770		0.13			
Yb	0.168	0.971	3.028	17.50	2.28	0.61	29.2	48	580
Lu	0.0246	0.141	0.438	2.503	0.34	0.07	4.26	8.6	90.4
$La_{CI}/La_{CI}*^g$	1	1	0.88	0.88	0.68	1.33	1.20	1.84	1.52
$Ce_{CI}/Ce_{CI}*^g$	1	1	0.94	0.94	0.88	0.71	2.22	1.01	1.09
$La_{CI}/La_{CI}*^1$	1	1	1.10	1.10	0.91	1.57	1.33	1.89	1.71
$Ce_{CI}/Ce_{CI}*^1$	1	1	1.02	1.02	0.95	0.74	2.31	1.02	1.14
$La_{SN}/La_{SN}*^g$	1.13	1.13	1	1	0.76	1.51	1.35	2.09	1.72
$Ce_{SN}/Ce_{SN}*^g$	1.06	1.06	1	1	0.94	0.75	2.36	1.08	1.15
$La_{SN}/La_{SN}*^1$	2.71	2.71	1	1	-0.46	-1.42	1.42	-28.69	1.77
$Ce_{SN}/Ce_{SN}*^1$	1.26	1.26	1	1	2.27	1.43	2.40	1.47	1.17

614
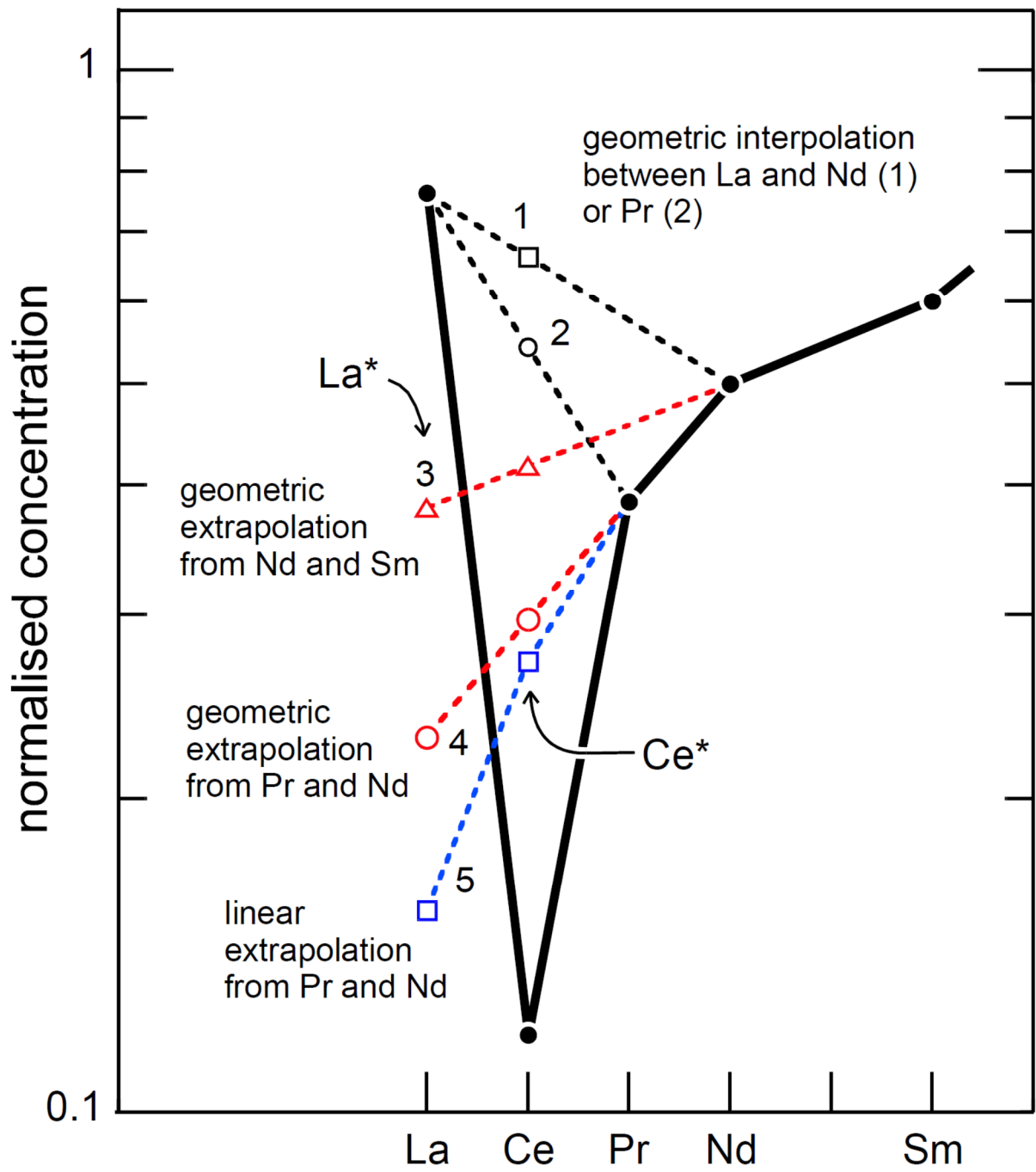
615
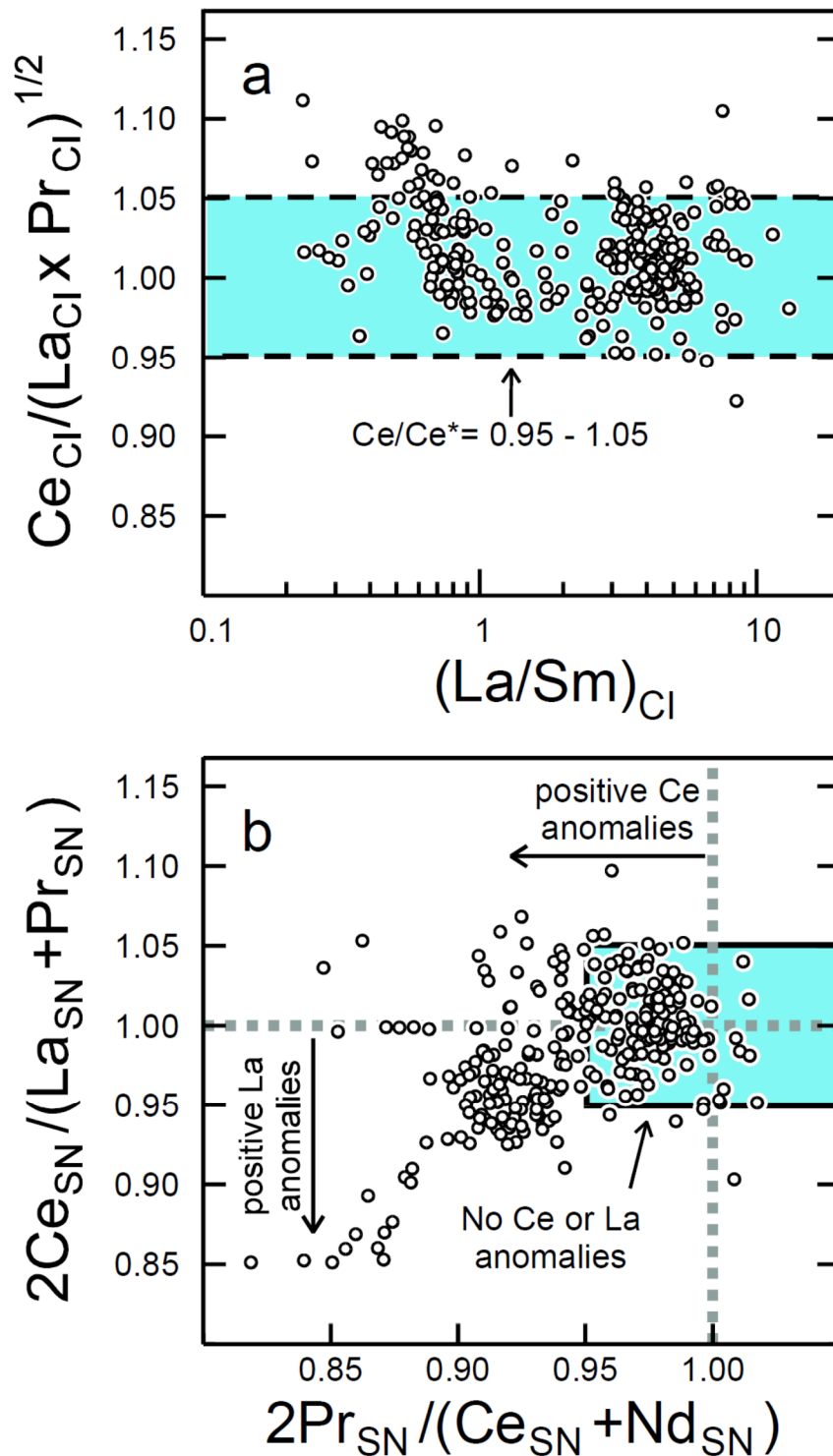616

617   Figure 1. The different ways of calculating La* and Ce*.

618

619

620

621

Figure 2. The 286 samples devoid of La and Ce anomalies of the database used to compare linear and geometric extrapolations for calculating La* and Ce*, are plotted in a Ce/Ce* vs. La/Sm plot (a) and in the Ce/Ce* vs. Pr/Pr* plot of Bau and Dulski (1996a) (b). Ce* is geometrically interpolated in (a) and linearly interpolated in (b).
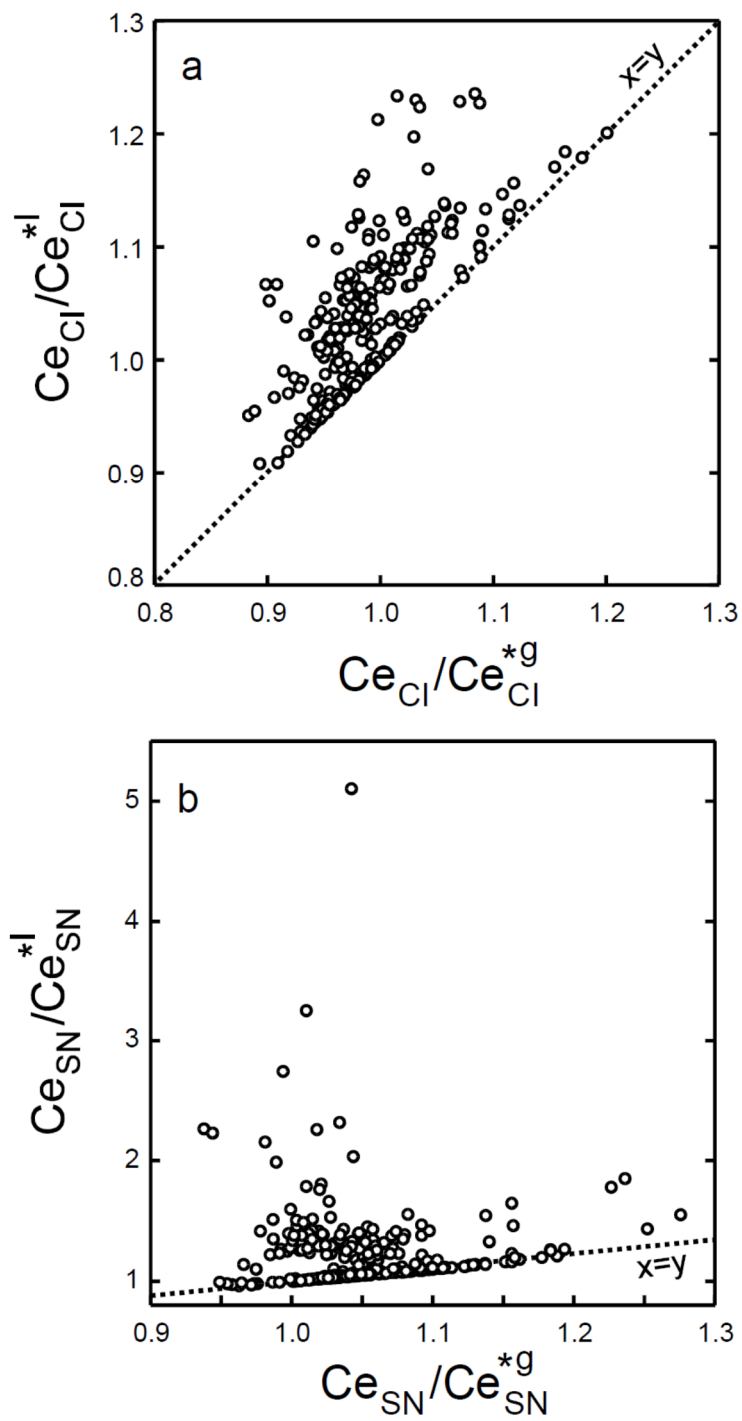
626

627

628

629
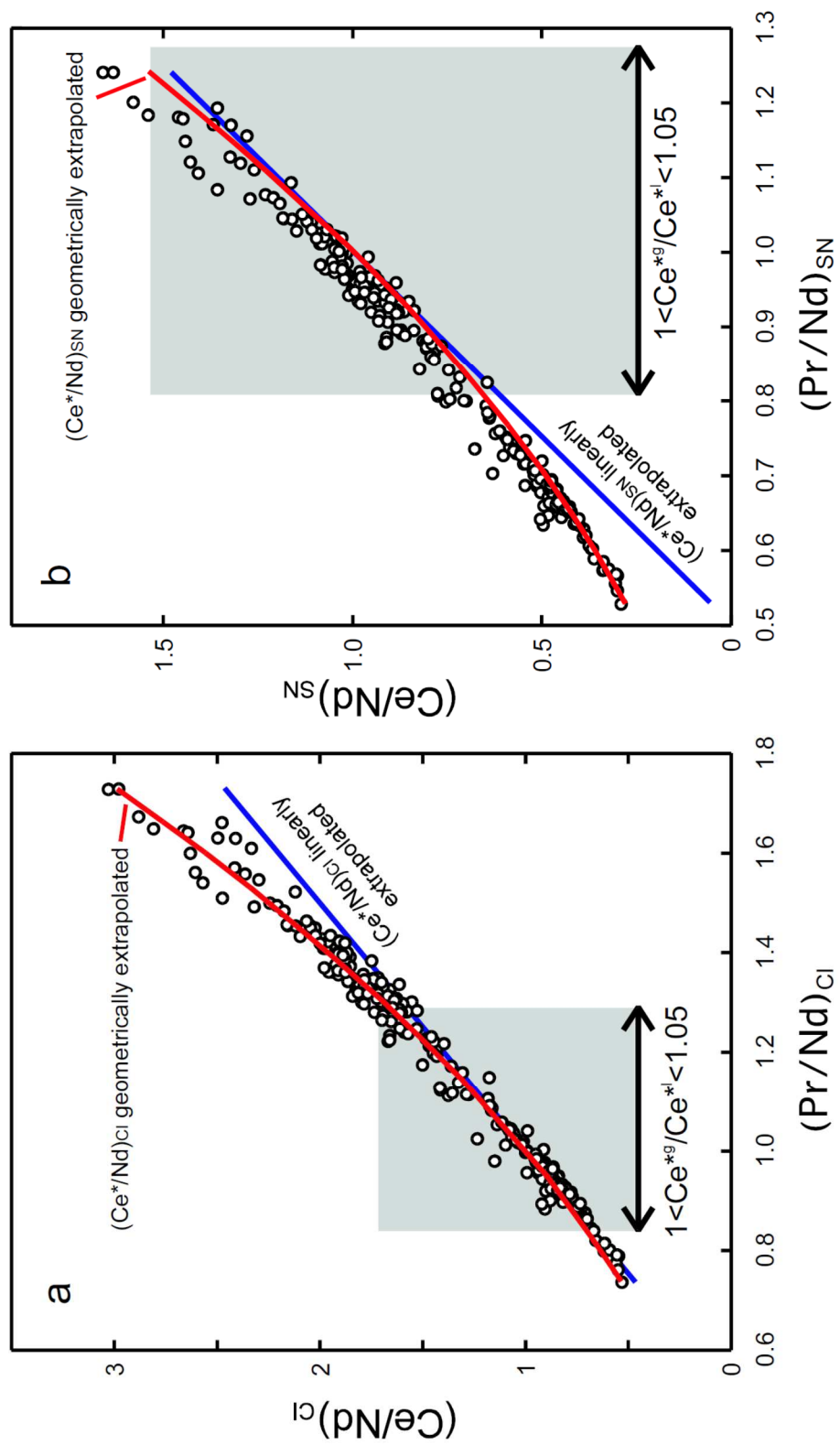
Figure 3. Ce/Nd vs. Pr/Nd plots for the samples devoid of La and Ce anomalies of our database, used here to compare linear (blue line) and geometric (red parabola) extrapolations for Ce*. The data are normalized with CI chondrite (a) or with PAAS (b).

633

634

Figure 4. $Ce_{CI}/Ce_{CI}*^l$ vs. $Ce_{CI}/Ce_{CI}*^g$ (a) and $Ce_{SN}/Ce_{SN}*^l$ vs. $Ce_{SN}/Ce_{SN}*^g$ (b) plots for the samples devoid of Ce anomalies used to test the different extrapolations. Notice the ranges of values obtained.

638

639

640

641

642

643

644
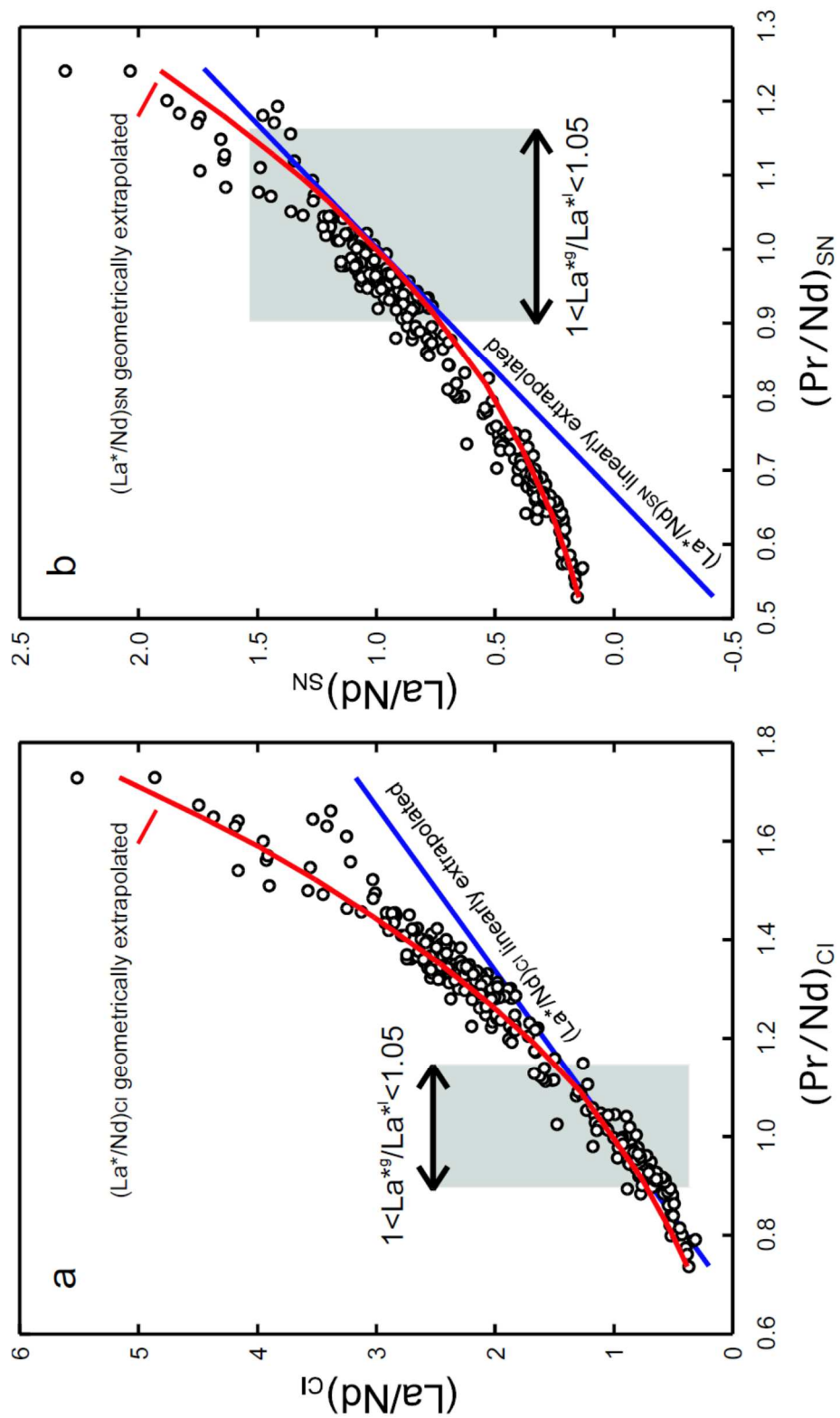
Figure 5. La/Nd vs. Pr/Nd plots for the samples devoid of La and Ce anomalies of our
database used to compare linear (blue line) and geometric (red cubic) extrapolations for Ce*.
The data are normalized with CI chondrite (a) or with PAAS (b).
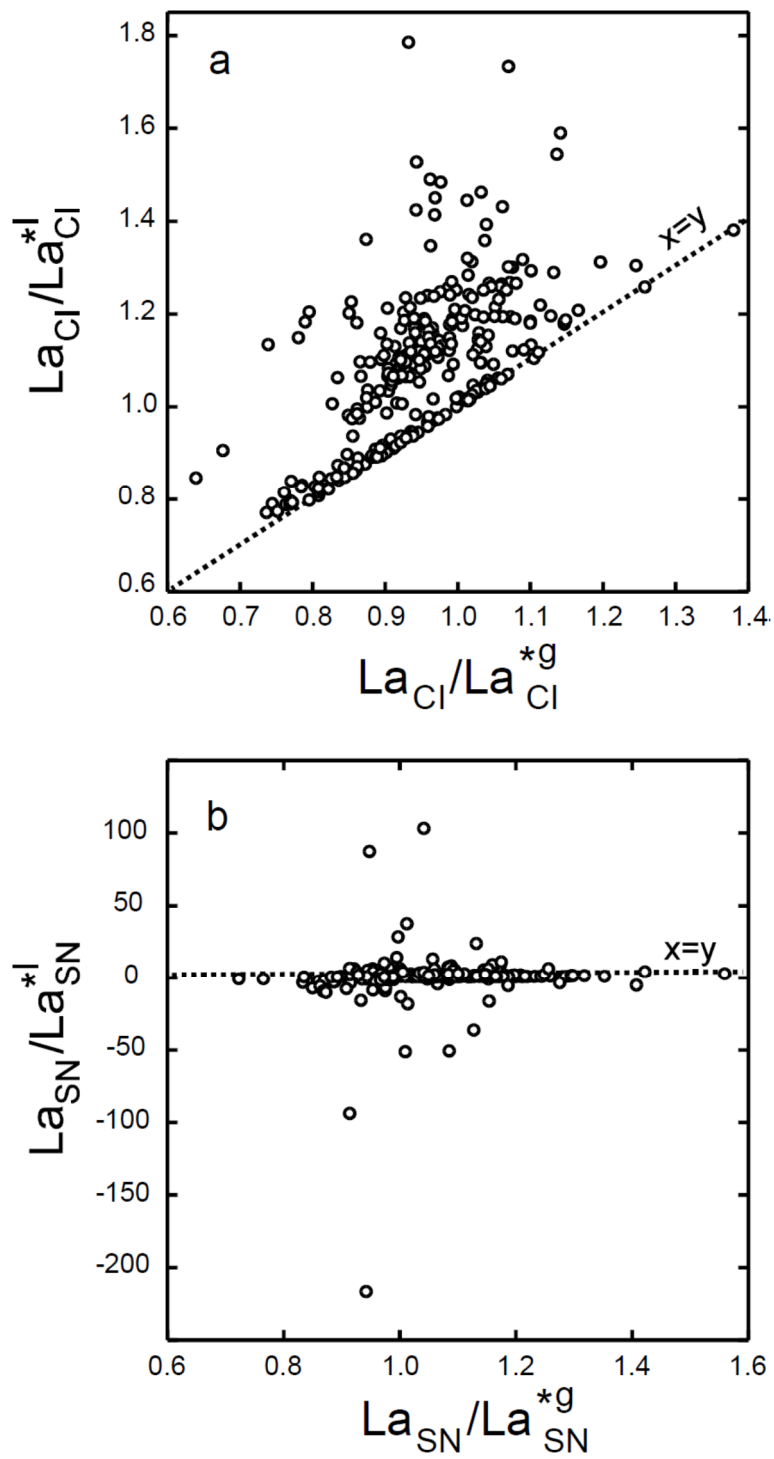
Figure 6. La_{CI}/La_{CI}^{*l} vs. La_{CI}/La_{CI}^{*g} (a) and La_{SN}/La_{SN}^{*l} vs. La_{SN}/La_{SN}^{*g} (b) plots for the samples devoid of La anomalies used to test the different extrapolations. Notice the ranges of values obtained.

656

657

658
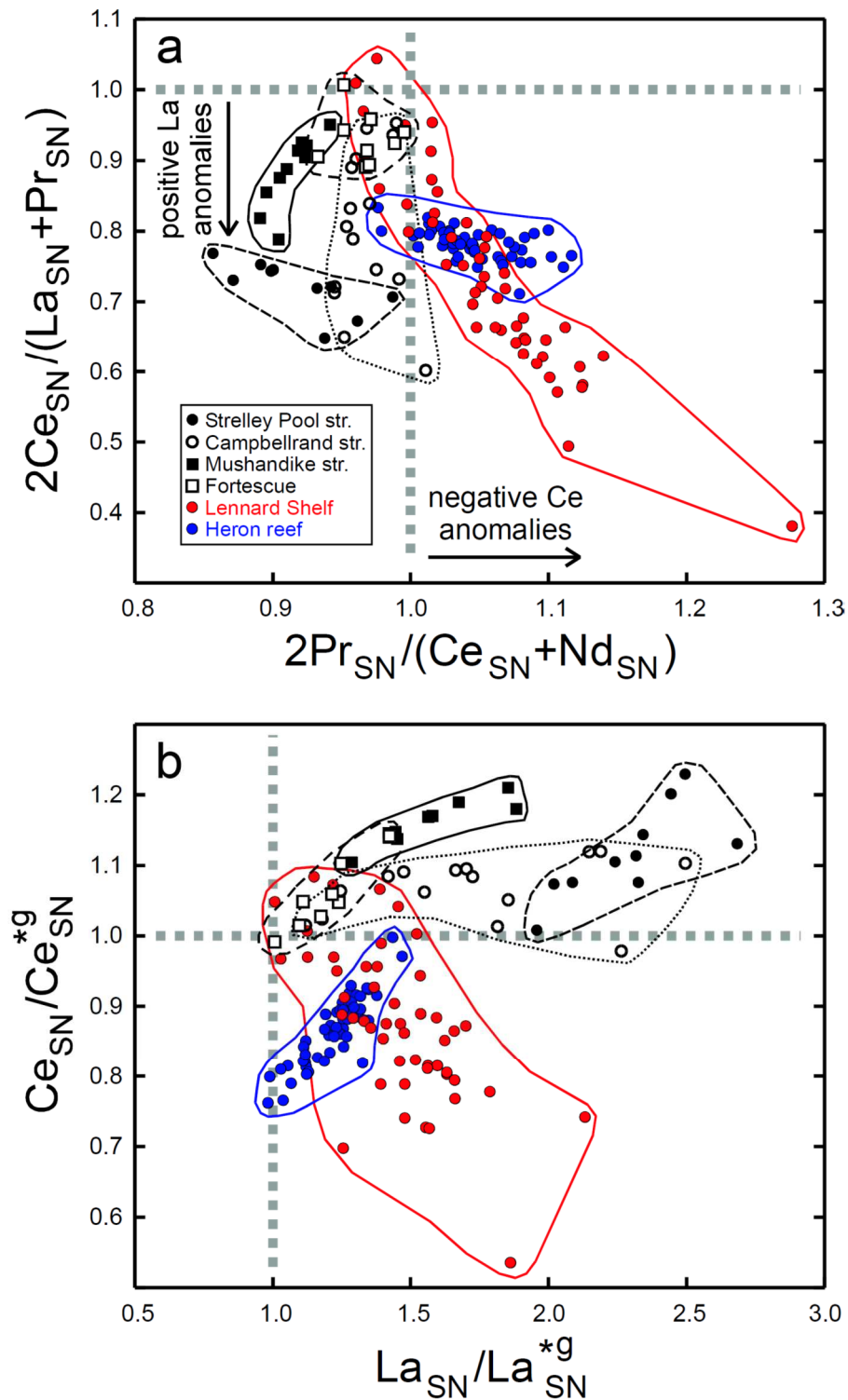
Figure 7. Selected carbonates are plotted in the Ce/Ce* vs. Pr/Pr* plot of Bau and Dulski
(1996a) (a) where Ce* and Pr* are linearly interpolated, and in a Ce/Ce* vs. La/La* where
Ce* and La* are geometrically extrapolated. Notice the different Ce/Ce* ranges obtained. See
text for more details.
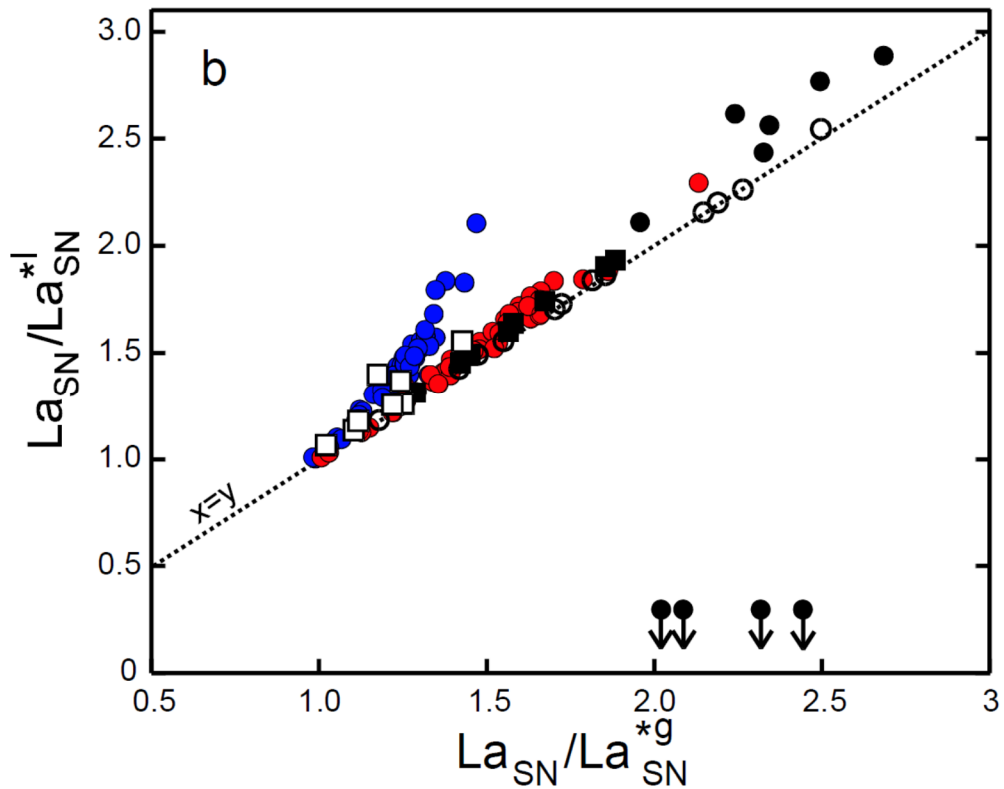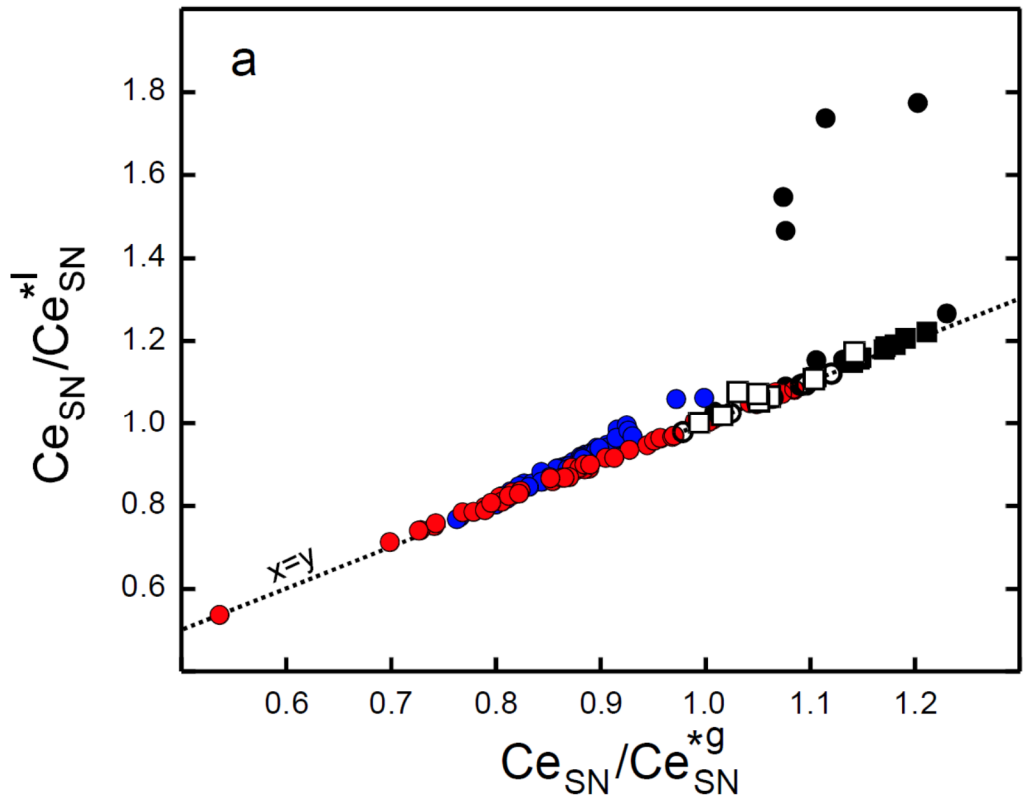
Figure 8. Ce_{SN}/Ce_{SN}^{*l} vs. Ce_{SN}/Ce_{SN}^{*g} (a) and La_{SN}/La_{SN}^{*l} vs. La_{SN}/La_{SN}^{*g} (b) plots for the selected carbonates used to test the different extrapolations (same caption as Fig. 7).
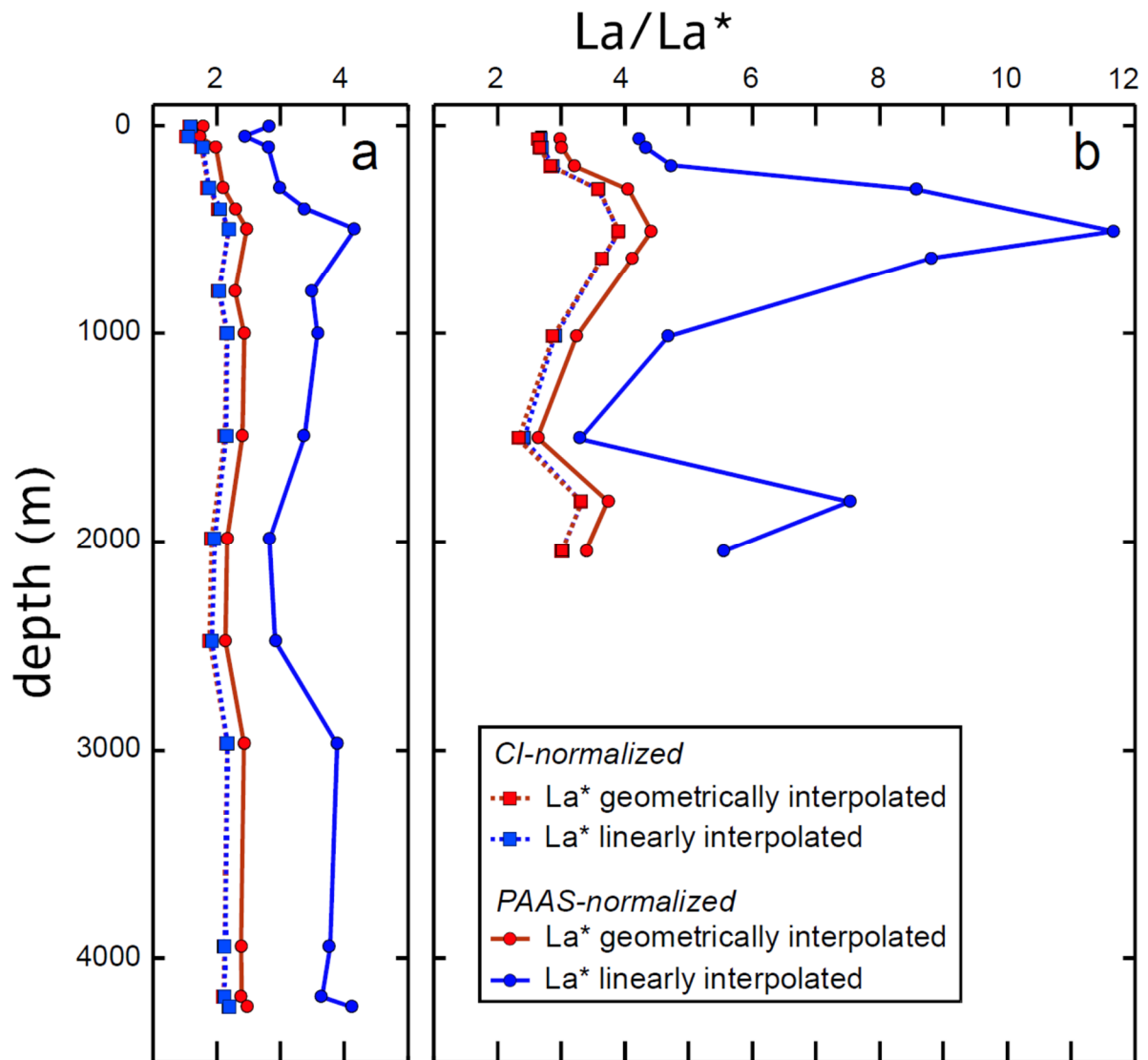
667

668
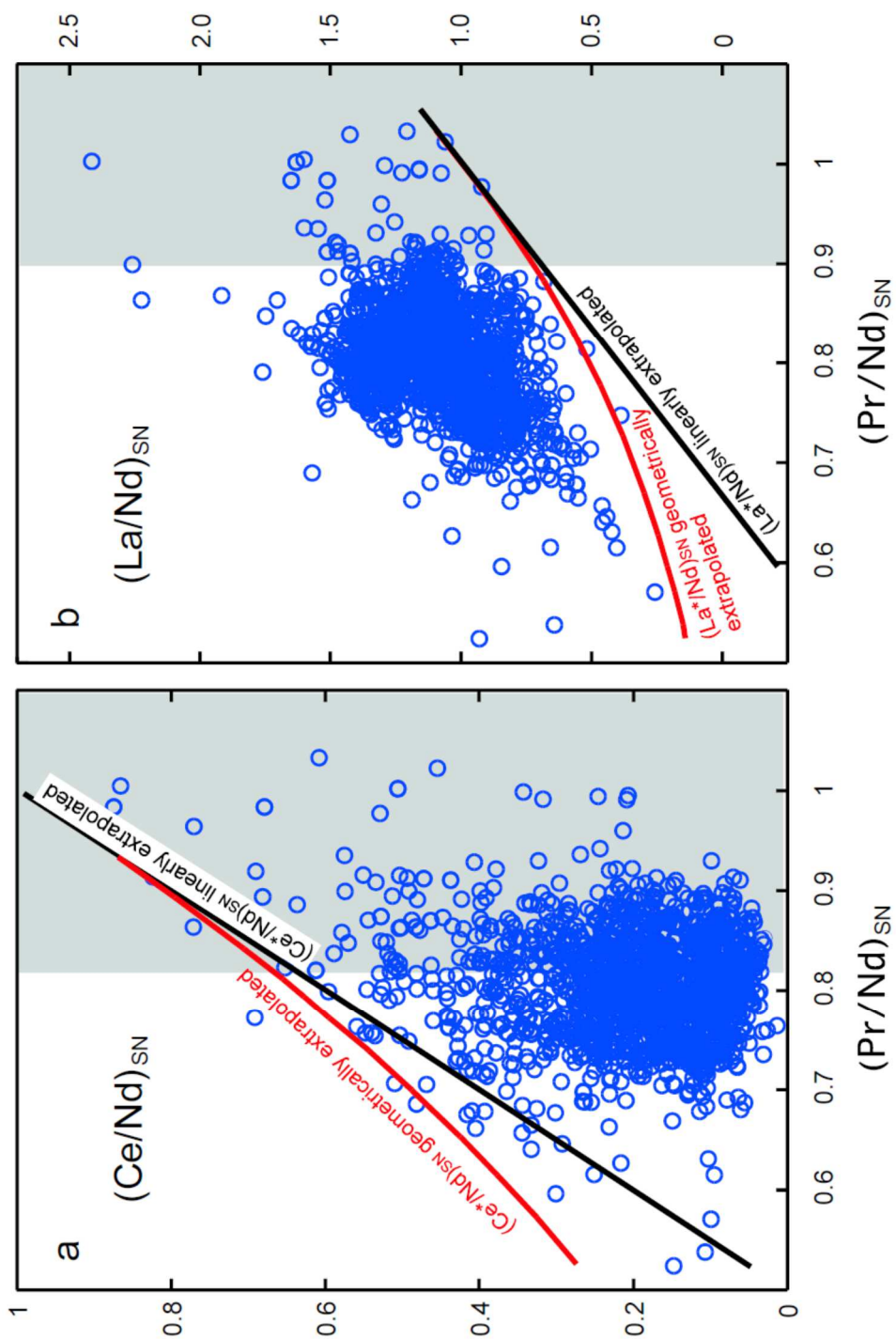
Figure 9. (Ce/Nd)$_{SN}$ (a) and (La/Nd)$_{SN}$ (b) vs. (Pr/Nd)$_{SN}$ plots for seawater. The shaded areas correspond to the range in Pr/Nd ratios for which the linear and geometric extrapolations are similar (1<X*l/X*g<1.05). A large proportion of the samples are outside the ranges where the linearly extrapolated Ce* or La* are equivalent to the geometrically extrapolated ones.

673

674

Figure 10. Vertical profiles of La anomaly (La/La*) at (a) station PA-11, South China Sea (February 11 and 12, 1997; 15°22'N, 115°17'E; depth: 4240 m ; Alibo and Nozaki, 2000) and at (b) the meander core station E1, Kerguelen Plateau (October 30, 2011; 72.178°E, 48.498°S; depth: 2058 m, Grenier et al., 2018). La/La* was calculated linearly and geometrically with data normalized with chondrite or with PAAS. The $La_{SN}/La_{SN}*^{1}$ values are always much larger than the other La/La* estimates, and is an artifact.